Publications

6-5-2007

Simulated Ducting of High-frequency Atmospheric Gravity Waves in the Presence of Background Winds

Yonghui Yu
Embry-Riddle Aeronautical University

Michael P. Hickey Ph.D.
Embry-Riddle Aeronautical University, hicke0b5@erau.edu

Follow this and additional works at: https://commons.erau.edu/publication

Part of the Atmospheric Sciences Commons

Simulated ducting of high-frequency atmospheric gravity waves in the presence of background winds

Yonghui Yu[1,2] and Michael P. Hickey[1,2]

[1] A new nonlinear and time-dependent model is used to derive the total perturbation energy flux of two gravity wave packets propagating from the troposphere to the lower thermosphere. They are excited by a heat source and respectively propagate in an eastward and westward direction in the presence of a zonal wind. Analysis of the refractive index, the power spectra and the total perturbation energy flux allows us to correctly interpret the ducting characteristics of these two wave packets. In our study the wind acts as a directional filter to the wave propagations and causes noticeable spectral variations at higher altitudes. We are the first that time-resolve the total perturbation energy flux influenced by the winds and the simulations have immediate impacts to the airglow observations on certain wave spectra. **Citation:** Yu, Y., and M. P. Hickey (2007), Simulated ducting of high-frequency atmospheric gravity waves in the presence of background winds, *Geophys. Res. Lett.*, *34*, L11103, doi:10.1029/2007GL029591.

1. Introduction

[2] Upward propagating gravity waves in the atmosphere are highly influenced by the thermal structure [*Walterscheid et al.*, 1999] and the background winds [*Hecht et al.*, 2001]. For high-frequency gravity waves the possibility of trapping and ducting arises wherein a local region of propagation is sandwiched between two regions of evanescence. Alternatively, ducting can also occur in a region of propagation between the ground and a higher region of evanescence. In the case of thermal ducting the region of propagation occurs in the vicinity of a local maximum in the Brunt-Väisälä frequency. The inclusion of winds with shears will cause a height-dependent Doppler shift of wave frequencies for the wave propagation with a component parallel to the wind, which may either reinforce or destroy the ducting depending on the properties of the waves and the winds. The ducting that is facilitated by mean winds is commonly referred to as Doppler ducting. Observations in the airglows and simulations from models verify that atmospheric gravity waves may be thermally ducted [*Hecht et al.*, 2001; *Hickey*, 2001; *Walterscheid et al.*, 1999, 2001; *Snively and Pasko*, 2003; *Yu and Hickey*, 2007a, 2007b] and Doppler-ducted [*Isler et al.*, 1997; *Walterscheid et al.*, 1999; *Hecht et al.*, 2001; *Hickey*, 2001; *Snively et al.*, 2007].

[3] *Isler et al.* [1997] examined airglow observations of gravity waves and with measurements of mean winds they were able to determine that ~75% of the observed waves were ducted or evanescent and the remainder was freely propagating. Quasi-monochromatic (QM) waves observed in airglow images were interpreted by *Walterscheid et al.* [1999] as waves ducted or trapped in the lower thermospheric thermal duct. *Hecht et al.* [2001] observed periodic structures of QM waves propagating horizontally and coherently across airglow images. They typically had horizontal wavelengths on an order of tens of kilometers and periods of several minutes. *Snively and Pasko* [2003] provided simulations of ducted gravity waves generated by nonlinear wave breaking in the far-field lower thermospheric thermal duct. Thermal ducting in the presence of multiple ducts (in the stratosphere, mesosphere and lower thermosphere) has been described in the modeling studies of *Yu and Hickey* [2007a, 2007b].

[4] The purpose of this paper is to study the effects of mean winds on the ducting of atmospheric gravity waves by analysis of the time-resolved and horizontally averaged total perturbation energy flux, $\overline{p'w'}$ plus $\rho_0 \, \overline{U} \overline{u'w'}$ (which will be described in the Theory section). A spectral analysis of the time series of the vertical velocity is performed at discrete altitudes to help quantify the wave trapping and ducting. A 2-D nonlinear and time-dependent model (the AGE-TIP model is described by *Yu and Hickey* [2007a, 2007b]) is used in the current simulations.

2. Theory

[5] The dispersion relation [*Hines*, 1960] can involve the thermal and wind effects in a WKB approximation [*Einaudi and Hines*, 1971] and can be solved for the squared vertical wave number (m^2) that is given by

$$m^2 = \frac{(N^2 - \Omega^2)}{\Omega^2} k^2 + \frac{(\Omega^2 - \omega_a^2)}{C^2}. \qquad (1)$$

Here $\Omega = \omega - \underline{k} \cdot \underline{\bar{U}}$ is the intrinsic (Doppler-shifted) frequency, ω is the extrinsic (ground-based) frequency, $\underline{k}$ is the horizontal wave number vector, $\underline{\bar{U}}$ is the horizontal mean wind vector, C is the sound speed, N is the Brunt-Väisälä frequency, and ω_a is the acoustic-cutoff frequency. The effects of wind shears are implicitly included in (1) since $\Omega = \omega - \underline{k} \cdot \underline{\bar{U}}$. The effects of thermal gradients are in the definition of the non-isothermal Brunt-Väisälä frequency, $N^2 = g \, d \ln \theta/dz = (\gamma - 1 + \gamma dH/dz)g^2/C^2$, where g is the gravitational acceleration, γ is the ratio of specific heats, H is the atmospheric scale-height, and θ is the potential temperature [*Einaudi and Hines*, 1971]. For

[1]Department of Physical Sciences, Embry-Riddle Aeronautical University, Daytona Beach, Florida, USA.
[2]Department of Physics, University of Central Florida, Orlando, Florida, USA.

internal acoustic and gravity waves $m^2 > 0$, while for evanescent waves $m^2 < 0$. The m^2 varies with height in the atmosphere and so upward propagating waves can be internal at some heights and evanescent at others. Height-dependent winds Doppler shift the waves so that their intrinsic frequencies (Ω) also vary with height. Waves propagating with a component in a direction opposite to the wind will be Doppler-shifted to higher frequencies so that their m^2 decreases and the internal waves may become evanescent. Waves propagating with a component in the same direction as the wind will be Doppler-shifted to lower frequencies so that their m^2 increases and the evanescent waves may become internal. Therefore the combinations of height-dependent winds and mean temperature determine wave ducting [*Walterscheid et al.*, 1999; *Hecht et al.*, 2001; *Hickey*, 2001].

[6] Here we study wave propagation and ducting in a non-isothermal and windy atmosphere using the 2-D AGE-TIP model [*Yu and Hickey*, 2007a, 2007b]. Briefly, the model solves the Navier-Stokes equations including eddy and molecular processes. A sponge layer applies near the upper boundary and periodic boundary conditions apply at the lateral boundaries (separated by a horizontal wavelength) to simulate a horizontally infinite domain. The horizontal and vertical grids are 0.5 and 1.0 km, respectively. The time step is 0.7 sec. We specifically examine the different propagation characteristics between eastward and westward propagating wave packet with a zonal wind.

[7] In an atmosphere free of dissipation the vertical energy flux [*Yu and Hickey*, 2007a] is not a conserved quantity for gravity waves propagating through regions of wind shear. A form of the total perturbation energy flux that is conserved in this circumstance is given as [*Hines and Reddy*, 1967; *Hickey and Brown*, 2002]

$$F_T = \overline{p'w'} + \rho_0 \overline{U} \overline{u'w'}. \qquad (2)$$

(2) demonstrates how the momentum flux (e.g., $\rho_0 \overline{u'w'}$) contributes to the F_T. The contribution can be thought of as a consequence of a coupling between the waves and the mean flow [*Hines and Reddy*, 1967]. The F_T will be used while we are considering a time-dependent wave packet with myriad frequency components. We will designate the momentum flux contribution to the F_T as F_C.

3. Results

[8] The mean atmospheric thermal and density structures and winds are respectively defined by the MSIS-E-90 model [*Hedin*, 1991] and the Horizontal Wind Model (HWM93) [*Hedin et al.*, 1996]. Simulations are performed for the date of 1993 Jan 15 at 18.5°N latitude and 0.0° longitude and for the local time of 2200 hrs. The solar and geomagnetic indices are $F_{10.7} = F_{10.7A} = 87$ and $a_p = 12$ for moderately disturbed conditions. An eastward propagating wave packet with a primary period of 6.276 min and a horizontal wavelength of 35 km is used here and also in previous studies [*Yu and Hickey*, 2007a, 2007b]. These parameters were first determined using a full-wave model to study a strongly ducted gravity wave in the lower thermospheric thermal duct for a windless atmosphere [*Hickey*, 2001]. The

eastward propagating wave packet is excited by a heat source Q_w as

$$Q_w(x,z,t) = 10^{-5} \exp\left(-(t-\tau)^2/2\Delta t^2\right)$$
$$\cdot \exp\left(-(z-\xi)^2/2\Delta z^2\right) \sin(k_0 x - \omega_0 t), \qquad (3)$$

where $\Delta z = 0.8$ km, $\xi = 8$ km, $\Delta t = 6.276$ min, and $\tau = 37.656$ min. The forcing horizontal wave number and frequency are given by $k_0 = 2\pi/35$ km and $\omega_0 = 2\pi/6.276$ min, respectively. The forcing amplitude is chosen to be 10^{-5} (K s^{-1}) so that the resulting wave amplitude remains small at all heights. Interference effects between waves are linear. An expression similar to (3) but with a negative sign in the k_0 is used to force a westward propagating wave packet.

[9] The Brunt-Väisälä frequency and the mean zonal wind (positive eastward) are shown in Figure 1 (left). The refractive indices (m^2) calculated using (1) for eastward and westward propagation are also shown in Figure 1 (right). The zonal wind (Figure 1, left) is predominantly eastward, except in narrow regions near 45 and 100 km altitude where it is westward with a value of $\sim$15 m s^{-1}. At $\sim$75 and 115 km altitude the zonal wind is a local maximum (eastward). It tends to monotonously increase with height above $\sim$135 km altitude. The eastward propagating waves (e.g., the 7.06 min wave) tend to be internal ($m^2 > 0$) at most heights. The shorter period components are exception and exhibit regions of weak evanescence near 50 and 90 km altitude (e.g., the 5.51 min wave). Based on the m^2 profile for the 5.51 min wave we would expect it to be weakly trapped in the stratosphere and also in the mesosphere. The westward propagating waves (e.g., the 6.31 min wave) are evanescent ($m^2 < 0$) in most of the mesosphere, and they are internal in the stratosphere ($\sim$15 to 50 km altitude) and also in the uppermost mesosphere and lower thermosphere ($\sim$90 to 120 km altitude). Based on the m^2 profile for the 6.31 min wave we would expect it to be strongly trapped in the stratosphere. The longer period westward propagating waves (e.g., the 9.58 min wave) remain internal at most heights.

[10] The normalized power spectra that are derived from the time series of the vertical velocities at altitudes of 8, 30 and 80 km and also derived from the thermal source function (3) (all sampled for $\sim$6 hrs) are shown in Figure 2 (left (eastward) and right (westward)). These spectra have been adjusted for the Doppler shifting due to the mean winds to help facilitate a meaningful comparison amid spectra at different altitudes and between different orientations. The adjusted frequency ω^* is in the moving reference frame of the source altitude (8 km), $\omega^* = \Omega + \underline{k}(\overline{U}(z) - \overline{U}_s)$, where $\overline{U}_s$ is the zonal wind at $z = 8$ km. All other variables are so defined. The frequency ω^* is not the extrinsic frequency observed on the ground. For clarity, the spectra are normalized to be fractions of the sum of all power spectral amplitudes at each altitude. Our intent is to emphasize the frequency content at each altitude.

[11] For the westward propagating waves (Figure 2, right) the spectra are dominated by shorter period components in the stratosphere (e.g., the 30 km green curve). Longer period components are seen in the upper mesosphere spectra (e.g., the 80 km blue curve) but shorter period components
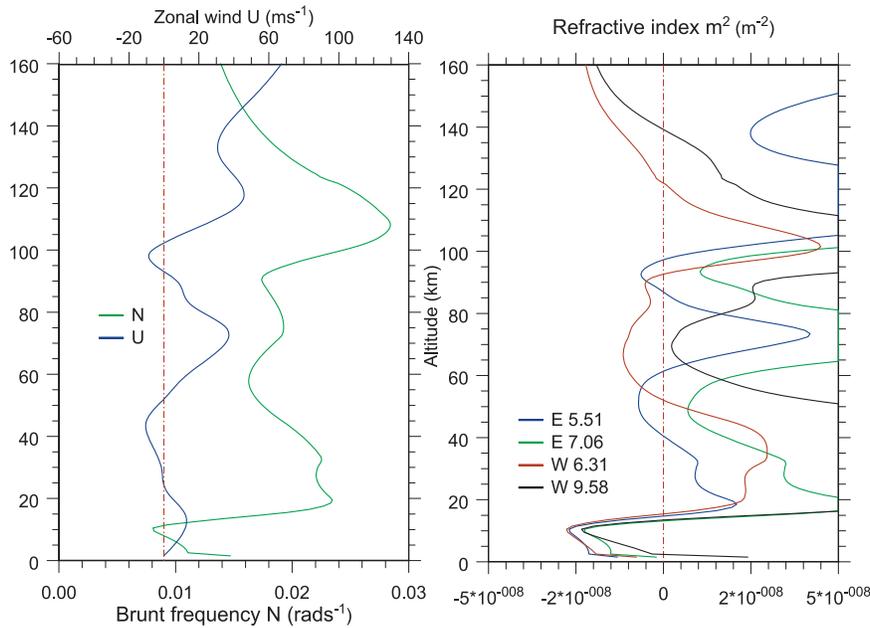
Figure 1. Atmospheric stability (*N*, green) and zonal wind (*U*, blue) are shown (left). The refractive indices, m^2, for wave periods of 5.51 min (E 5.51, blue) and 7.06 min (E 7.06, green) in eastward propagation, and for wave periods of 6.31 min (W 6.31, red) and 9.58 min (W 9.58, black) in westward propagation are also shown (right). The vertical line (dash-dot) signifies $U = 0$, (left) and m = 0 (right).

are absent due to their efficient trapping in the stratosphere, as discussed previously with respect to the refractive indices. Because the source spectrum (the black curve) does not efficiently generate the longer period waves, very little wave energy reaches the upper mesosphere for westward propagation. For the eastward propagating waves (Figure 2, left) the spectra are demonstrated by longer and shorter period

components in the stratosphere (e.g., the 30 km green curve) and by shorter period components in the upper mesosphere (e.g., the 80 km blue curve). Examination of the refractive index curves (Figure 1, right) shows that the longer period components (e.g., the 7.06 min wave) remain internal at most heights. These longer period components freely propagate through the mesosphere, and so do not substantially
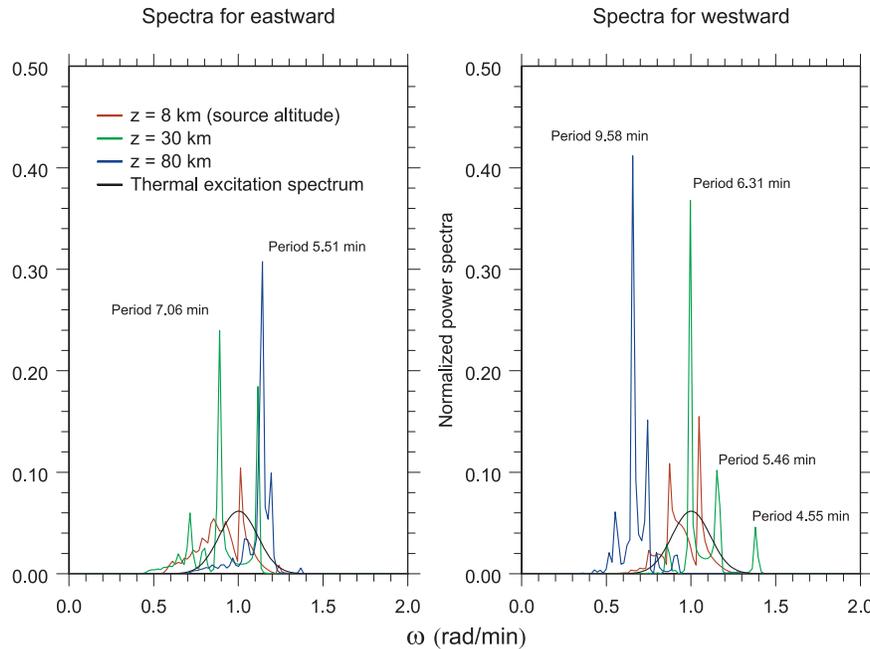

Figure 2. Wave spectra derived from the time series of the vertical velocities are shown for eastward propagation (left) and westward propagation (right) at discrete altitudes of 8 km (red), 30 km (green), and 80 km (blue). The spectrum derived from the thermal source function at 8 km altitude is also shown (black).
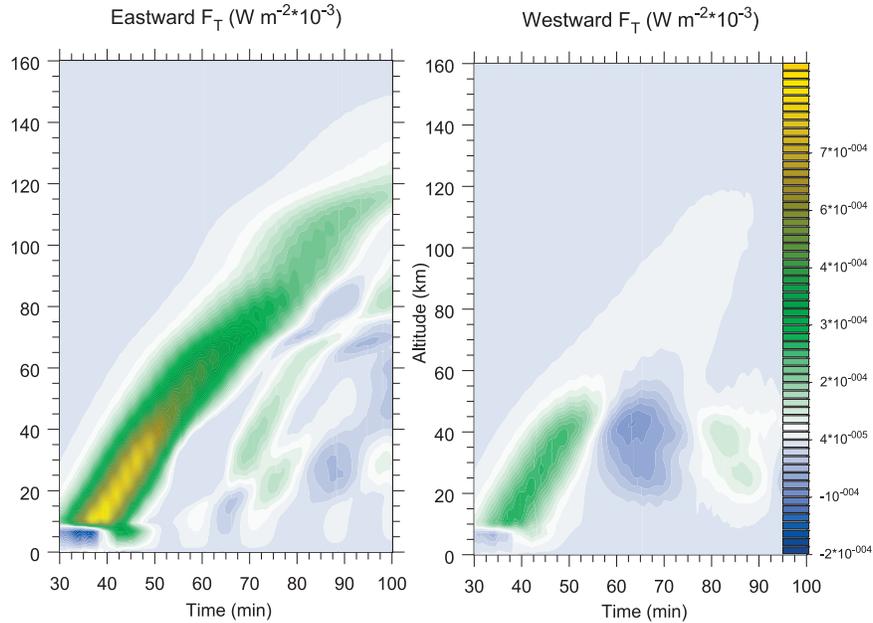
Figure 3. The total perturbation energy flux F_T (W m^{-2}) is shown for eastward (left) and westward (right) propagation.

contribute to the spectrum that is based on a time series of $\sim$6 hrs. Shorter period components of the eastward propagating waves (e.g., the 5.51 min wave) have regions of weak evanescence near 50 and 90 km altitude. This wave is weakly trapped and ducted near 25 and 75 km altitude. Therefore, it spends more time in these regions than it would if it was freely propagating and so locally dominates the spectra (both in the 30 km green and 80 km blue curves).

[12] The F_T calculated with (2) is shown as a function of time and altitude in Figure 3 (left (eastward) and right (westward)). As the eastward propagating wave packet propagates upward from the troposphere it weakens, significantly so near 50 and again near 90 km altitude. The longer period components are able to reach the upper mesosphere and lower thermosphere essentially unimpeded because they remain internal at most heights (see Figure 1, right). The regions of significant weakening of the F_T correspond to regions where $m^2 < 0$ for shorter period components of the wave packet. The zonal wind impedes the propagation of the shorter period components to higher altitudes by Doppler shifting them to evanescence within certain altitude ranges. This leads to the partial trapping of wave energy near the upper mesosphere and within the stratosphere. In so doing, it leads to large spectral signatures of these waves at 30 and 80 km altitude (Figure 2, left).

[13] The F_T for the westward propagating wave packet is shown in Figure 3 (right). The zonal wind significantly impedes the propagation of the westward propagating wave packet into the mesosphere, and most of the energy remains strongly trapped in the stratosphere. The small amount of energy reaching the upper mesosphere and lower thermosphere ($\sim$10% of the original wave energy) resides mainly in the longer period components in the spectrum ($\sim$7– 13 min), as discussed in relation to Figure 2 (right). A long period ($\sim$40 min) variation of the F_T is seen to occur in the stratosphere, as identified by the alternating direction of the

F_T in Figure 3 (right). As discussed by *Yu and Hickey* [2007a], such variation is associated with the finite time taken for reflections between the lower and upper duct boundaries, which in turn depends on the vertical group velocity of ducted waves.

[14] In Figure 4 we show the contribution of the momentum flux (F_C) to the F_T. As the eastward propagating waves (Figure 4, left) propagate upward, F_C changes sign with the changes in the direction of the zonal wind (see (2) and Figure 1, left). When the zonal wind is eastward as the same direction as the propagating waves, the waves extract energy from the mean flow, whereas when the zonal wind is westward as the opposite direction to the propagating waves, the waves deposit energy to the mean flow [e.g., *Hines and Reddy*, 1967]. F_C changes sign as time increases at fixed altitudes (e.g., $\sim$40 and 70 km, Figure 4, left) due to partial reflections of the wave packet and the associated sign changes of the momentum flux. In the upper troposphere and the lower stratosphere F_C contributes $\sim$20% to the F_T, but in the lower thermosphere it contributes up to 40% to the F_T because of the large zonal wind in this region ($\sim$60 m s^{-1} at $\sim$160 km altitude, Figure 1, left). For the westward propagating waves (Figure 4, right) F_C is significant only in the stratosphere (e.g., 40 km altitude) due to wave trapping, and it changes sign with increasing time due to reflections and the associated sign changes of the momentum flux. Comparison of Figure 4 (left and right) shows that at a particular time and altitude (e.g., 50 min, 40 km) F_C has the opposite sign for the eastward and westward propagating wave packet due to their momentum fluxes being oppositely directed.

4. Discussion

[15] Besides the energy flux, the vertical velocity is also a good indicator of the extent of the ducting region [*Snively and Pasko*, 2003; *Snively et al.*, 2007; *Yu and Hickey*,
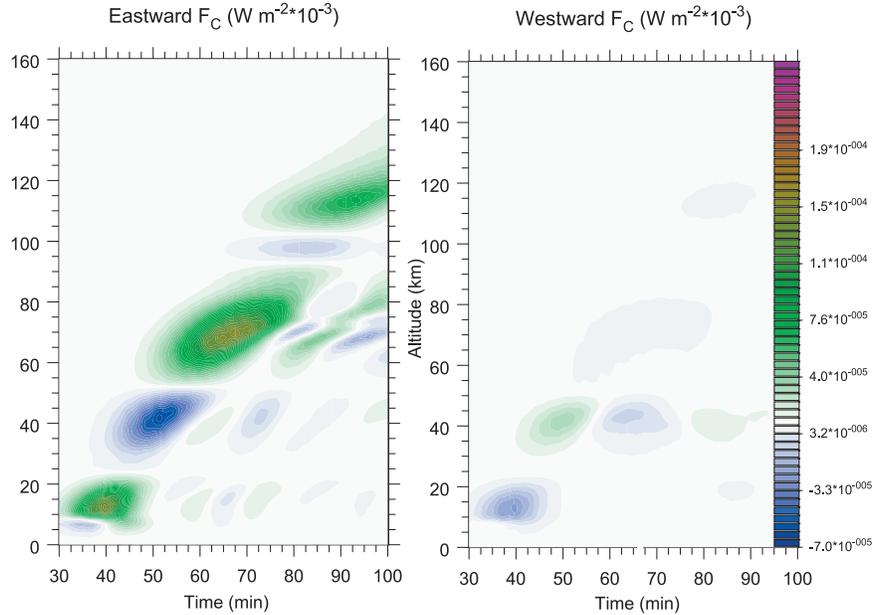
Figure 4. The contribution of the momentum flux F_C (W m^{-2}) is shown for eastward (left) and westward (right) propagation.

2007b]. We note that the Gaussian wave train in (3) is too short to fill the entire vertical extent of the atmosphere leading to incomplete cancellation of the upward and downward propagating waves. Hence fully ducted waves aren't generated. If complete cancellation had been achieved then the energy flux would have approached zero once the waves filled the ducting region, while the vertical velocity would exhibit node(s) and antinode(s) [*Yu and Hickey*, 2007a].

[16] *Hecht et al.* [2001] studied the propagation of QM waves in the atmosphere and showed that waves having a certain direction of propagation are more favorably ducted in the lower thermospheric thermal duct and therefore observable in the nightglows. For other directions of propagation, they found that large regions of evanescence in the middle atmosphere inhibited the propagation of the waves to the lower thermosphere. Here we have considered the propagation of a fairly high frequency wave packet through a moving background atmosphere, and found that certain wave components are inhibited from propagating to the lower thermosphere. For the eastward propagating wave packet the spectrum at 80 km altitude is dominated by the shorter period components ($\sim$5−6 min). This is because the longer period components are internal and propagate unimpeded through the upper mesosphere region quickly, with the result that their spectral signatures are small. The shorter period components of the eastward propagating waves undergo partial reflections and trapping, with the result that they spend more time in the stratosphere and in the upper mesosphere and so dominate the spectra in these regions.

[17] For the westward propagating wave packet the longer period components ($\sim$7−13 min) dominate the spectrum in the upper mesosphere, but the energy of these waves is considerably smaller than that of the eastward propagating waves. The downward propagating wave energy for the westward propagating wave packet seen at $\sim$65 min and

$\sim$40 km altitude in Figure 3 (right) is a sign of wave trapping in the stratosphere. The F_T alternates direction periodically in time as a result of reflections from regions of evanescence at the duct boundaries, leading to a long period ($\sim$40 min) fluctuation in the stratosphere. This phenomenon, also discussed by *Yu and Hickey* [2007a], continues for longer times (not shown) during which the trapped waves finally dissipate.

5. Conclusion

[18] We have simulated the propagation of two high-frequency gravity wave packets from the troposphere to the lower thermosphere in the presence of mean background winds. The westward propagating wave packet is largely trapped in the stratosphere and its alternating upward and downward energy fluxes are associated with reflections from the stratospheric duct boundaries. The longer period components of the eastward propagating wave packet propagate unimpeded and quickly through the atmosphere, while the shorter period components remain partially trapped near the airglow altitudes. Because these shorter period components of the eastward propagating wave packet spend more time in this region than that spent by the longer period components, they substantially contribute to the wave spectrum and would be more likely to be observed by optical techniques.

References

Einaudi, F., and C. O. Hines (1971), WKB approximation in application to acoustic-gravity waves, *Can. J. Phys.*, *48*, 1458−1471.

Hecht, J. H., R. L. Walterscheid, M. P. Hickey, and S. J. Franke (2001), Climatology and modeling of quasi-monochromatic atmospheric gravity waves observed over Urbana Illinois, *J. Geophys. Res.*, *106*, 5181–5196.

Hedin, A. E. (1991), Extension of the MSIS thermosphere model into the middle and lower atmosphere, *J. Geophys. Res.*, *96*, 1159–1172.

Hedin, A. E., et al. (1996), Empirical wind model for the upper, middle and lower atmosphere, *J. Atmos. Terr. Phys.*, *58*, 1421–1447.

Hickey, M. P. (2001), Airglow variations associated with nonideal ducting of gravity waves in the lower thermosphere region, *J. Geophys. Res.*, *106*, 17,907–17,918.

Hickey, M. P., and J. S. Brown (2002), A simulation study of space-based observations of gravity waves in the airglow using observed ALOHA-93 wave parameters, *J. Geophys. Res.*, *107*(A12), 1431, doi:10.1029/2001JA009225.

Hines, C. O. (1960), Internal atmospheric gravity waves at ionospheric heights, *Can. J. Phys.*, *38*, 1441–1481.

Hines, C. O., and C. A. Reddy (1967), On the propagation of atmospheric gravity waves through regions of wind shear, *J. Geophys. Res.*, *72*, 1015–1034.

Isler, J. R., M. J. Taylor, and D. C. Fritts (1997), Observational evidence of wave ducting and evanescence in the mesosphere, *J. Geophys. Res.*, *102*, 26,301–26,313.

Snively, J. B., and V. P. Pasko (2003), Breaking of thunderstorm-generated gravity waves as a source of short-period ducted waves at mesopause altitudes, *Geophys. Res. Lett.*, *30*(24), 2254, doi:10.1029/2003GL018436.

Snively, J. B., V. P. Pasko, M. J. Taylor, and W. K. Hocking (2007), Doppler ducting of short-period gravity waves by midlatitude tidal wind structure, *J. Geophys. Res.*, *112*, A03304, doi:10.1029/2006JA011895.

Walterscheid, R. L., J. H. Hecht, R. A. Vincent, I. M. Reid, J. Woithe, and M. P. Hickey (1999), Analysis and interpretation of airglow and radar observations of quasi-monochromatic gravity waves in the upper mesosphere and lower thermosphere over Adelaide, Australia (35°S, 138°E), *J. Atmos. Sol. Terr. Phys.*, *61*, 461–478.

Walterscheid, R. L., G. Schubert, and D. G. Brinkman (2001), Small-scale gravity waves in the upper mesosphere and lower thermosphere generated by deep tropical convection, *J. Geophys. Res.*, *106*, 31,825–31,832.

Yu, Y., and M. P. Hickey (2007a), Time-resolved ducting of atmospheric acoustic-gravity waves by analysis of the vertical energy flux, *Geophys. Res. Lett.*, *34*, L02821, doi:10.1029/2006GL028299.

Yu, Y., and M. P. Hickey (2007b), Numerical modeling of a gravity wave packet ducted by the thermal structure of the atmosphere, *J. Geophys. Res.*, doi:10.1029/2006JA012092, in press.

———————————

M. P. Hickey and Y. Yu, Department of Physical Sciences, Embry-Riddle Aeronautical University, Daytona Beach, FL 32114, USA. (michael.hickey@erau.edu; yonghui.yu@erau.edu)